Confirmation of X-ray Photoelectron Spectroscopy Peak Attributions of Nanoparticulate Iron Oxides, Using Symmetric Peak Component Line Shapes

ARTICLE *in* THE JOURNAL OF PHYSICAL CHEMISTRY C · MAY 2010

Impact Factor: 4.77 · DOI: 10.1021/jp100964x

4 AUTHORS, INCLUDING:

Suzie Poulin
Polytechnique Montréal
65 PUBLICATIONS **744** CITATIONS
SEE PROFILE

Rodrigo França
University of Manitoba
30 PUBLICATIONS **81** CITATIONS
SEE PROFILE

Confirmation of X-ray Photoelectron Spectroscopy Peak Attributions of Nanoparticulate Iron Oxides, Using Symmetric Peak Component Line Shapes

S. Poulin,[†] R. França,[‡] L. Moreau-Bélanger,[‡] and E. Sacher*,[†]

Regroupement Québécois de Matériaux de Pointe, Département de Génie Physique and Institut de Génie Biomédical, École Polytechnique, C.P. 6079, succursale Centre-ville, Montréal, Québec H3C 3A7, Canada

Received: February 1, 2010; Revised Manuscript Received: May 4, 2010

We use high purity Fe oxide nanoparticles to confirm the Fe 2p X-ray photoemission peak attributions made in our previous study of Fe nanoparticles and the initial stage of their oxidation. To accomplish this, we have found it necessary to consider the spectral contributions of the ligand field of the Fe−O crystal structure, the crystalline disorder at the nanoparticle surface, and the Russell−Saunders broadening of the Fe^{III} components of the Fe 2p spectra.

Introduction

In a previous paper,[1] our group used X-ray photoelectron spectroscopy (XPS) to characterize Fe nanoparticles (NPs). When permitted to undergo the initial stages of oxidation, by controlled exposure to O_2, we found that these nanoparticles gave rise to four new peaks in the Fe 2p spectrum, which we called C_1−C_4. Basing ourselves on prior results on Co nanoparticle oxidation,[2] as well as on our understanding of ligand field effects, we proposed, for the first time, the following oxidation scheme

$$Fe^0 + [O] \rightarrow FeO \text{ (rock salt structure)} \quad (1)$$

$$4FeO \rightarrow Fe^0 + Fe_3O_4 \text{ (inverse spinel structure)} \quad (2)$$

$$Fe_3O_4 + [O] \rightarrow \gamma\text{-}Fe_2O_3 \text{ (cubic close-packed structure)} \quad (3)$$

with the reaction in eq 1 being rate-controlling; our mechanism is supported by prior studies discussed in our paper.[1] This permitted us to attribute each of the four peaks to a given valence state (Fe^{II}, Fe^{III}) in a given crystal structure (rock salt, octahedral, tetrahedral). The purpose of the present work is to confirm these attributions, using highly pure Fe oxides whose structures are well established.

Over the years, there have been many studies of Fe and its oxides.[3−9] As we previously explained,[1] the existence of strikingly similar asymmetric 2p XPS spectra for Fe^0 *and its ions* eliminates the interpretations previously offered for the cause of this asymmetry: electron coupling (since the 2p spectral envelopes are different for Fe and its ions,[1,10] due to differing ground and excited states) and the asymmetry-predicting Doniach−Šunjić electron scattering process at the Fermi level[11] (since this applies only to metals and not to their compounds[1,11]).

Instead, we proposed[1] that the peak asymmetry is due to the vacancy cascade[12] previously proposed to occur in Fe; this process comprises a sequence of Auger electron and photon emissions, subsequent to inner-shell vacancy creation by initial electron photoemission. The result of this sequence of emissions is the creation of additional inner-shell vacancies, leading to further emissions. This composite process was the subject of a theoretical investigation by Jacobs et al.,[13,14] in the context of multiple ionizations following the creation of all energetically accessible inner-shell vacancies in a Fe atom and its ions. They found that such a vacancy cascade can be the prevailing mechanism for the production of multiple ionizations that would manifest themselves as XPS spectral contributions at binding energies higher than the main photoionization peak. Support for this attribution is found in the similar Auger emission probabilities calculated[14] for Fe^0 and its ions, which accounts for the similar 2p peak shapes found for Fe^0, its oxides, and halides.[6]

The present study uses XPS and X-ray diffraction (XRD) to chemically characterize the Fe oxides, along with particle size distribution measurements and scanning electron microscopy (SEM) to characterize them morphologically. We have also found it necessary to account, in our XPS spectra, for the differing ligand field effects of crystalline and disordered material, as well as for peak broadening due to Russell−Saunders (also called L−S or spin−spin) coupling.[15−17]

Experimental Section

Materials. The oxides used were of the highest purity and the smallest crystallite size readily available; all except the FeO were purchased from Alfa Aesar; they were α-FeO(OH) (#19496), Fe_3O_4 (#44120), α-Fe_2O_3 (#44666), and γ-Fe_2O_3 (#44896). The FeO was purchased from Sigma-Aldrich (#400866). All were reported to have purities greater than 99% and were used without further purification.

X-ray Diffraction. The crystallinities and mean crystal sizes of the NPs were determined from X-ray diffraction peaks of the powders deposited onto Al sample holders; this is a common method of NP characterization. The instrument used was a PANalytic X'Pert MPD, with Cu Kα radiation ($\lambda = 1.542$ Å), generated at 50 kV, 40 mA. The 2θ range of 15−80° was covered in 0.02° steps, and the diffraction patterns were analyzed using the X'Pert HighScore software accompanying the instrument, with comparisons against standards made using the stored JCPDS cards. Crystal dimensions were determined by the software, using the Scherer Equation, with c-Si as the correlation standard. The software was also capable of *suggesting* impurities, based on any existing extraneous peaks and improper peak height ratios.

* Corresponding author. E-mail: edward.sacher@polymtl.ca.
[†] Regroupement Québécois de Matériaux de Pointe.
[‡] Institut de Génie Biomédical.

10.1021/jp100964x
Published on Web 05/27/2010

Particle Size Distribution. The particle size distributions were determined by a Coulter LS Particle Size Analyzer, with the samples dispersed in methanol and sonicated, as instructed by the instrument manual. The instrument gives graphical outputs of the spherical equivalent of the volume, number, and surface areal percentages of the particles, over a spherical equivalent diameter size range of 0.4−2000 μm; it also calculates the statistics, including the diameter at which the mean value occurs, for each type of distribution.

Sample Morphology. Scanning electron microscopy was used to determine the sample morphology. Samples were deposited onto an amorphous carbon ribbon and inserted into a JEOL JSM-7600TFE scanning electron microscope. Images were obtained at a 2 keV accelerating voltage.

XPS. Chemical characterization was carried out on a VG ESCALab 3 Mk II, using nonmonochromated Al Kα radiation, at a power setting of 300 W, having an energy of 1486.6 eV and an instrument resolution of 0.85 eV. Samples were prepared by pressing the powders onto an adhesive Cu ribbon, completely covering the surface. No evidence of Cu was seen in the spectra; based on the fact that the C 1s spectrum obtained differed from that of the bare ribbon adhesive, contributions from the latter, too, may be excluded. Attempts to clean the samples with an Ar^+ beam led to significant sample loss through ion beam impact, and this was discontinued. The base pressure during scanning was below 1×10^{-9} Torr. Electrons were detected at a perpendicular takeoff angle, using steps of 0.05 eV, and spectra were analyzed using the VG Avantage software. The probe depth of the electrons is three times the electron attenuation length; for O 1s, the probe depth is ~3.5 nm and for Fe 2p, ~3 nm. The surface area analyzed was 2 mm × 3 mm.

Because a comprehension of our approach to peak separation is important to the understanding of our results, we give, here, a detailed description. High-resolution spectra were obtained for C 1s, O 1s, and Fe 2p. Peak separations, following Shirley background removal, were carried out in the following manner:

•The C 1s spectrum, which is due to a NP surface contaminant layer, was separated into peaks using a full width at half-maximum (fwhm) value of 1.6 eV, a value we have found applicable to such contamination layers; peak separation shows, as expected, both oxidized and nonoxidized components. This contaminant layer was initially deposited, during manufacture, on sample exposure to the atmosphere; the driving force was the lower surface energy of the contaminated surface (i.e., a reduction of Helmholtz free energy). The nonoxidized C 1s component (i.e., C−C), set at 285.0 eV, was used to calibrate the binding energy scale. In all the samples, this layer is sufficiently thin (estimated to be ≤1 nm) for the subsurface oxide to be clearly seen.

•The O 1s spectrum includes Fe−O (<532 eV) and oxidized C (>532 eV) components. The fwhm value for all peak components was fixed at 1.8 eV during peak separation. This is based on the fact that 25 years of experience with our XPS spectrometer, and hundreds of samples, have shown that this fwhm value is applicable to both organic and inorganic O. As will be explained, this certainty has permitted us to identify a component in the O 1s spectrum as due to structural disorder at the outer surfaces of the NPs.[18]

•The Fe 2p spectra manifest chemical shifts due to both the oxidation state (Fe^{II}, Fe^{III}) and the structural environment of the Fe (tetrahedral, octahedral), as well as contributions from the crystalline disorder at the outer surface of the NPs, as also found for O 1s.

•In addition, Fe^{III} undergoes a broadening due to Russell−Saunders coupling:[15−17] in the present case, this coupling occurs between the unpaired electron in the 3d orbital and the unpaired electron produced in the 2p orbital on photoemission. The coupling leads to six overlapping atomic states[15−17] (^{3}F, ^{1}F, ^{3}D, ^{1}D, ^{3}P, ^{1}P), at slightly different binding energies, whose overlap serves to broaden the peak, as we found for the similar case of Cu^{II}.[19] It is *a priori* impossible to separate the crystalline disorder and R−S contributions in the present case; thus, the widths used in the Fe 2p peak separations were those found for each oxide and contained both contributions.

•Each component of a multicomponent Fe 2p spectrum will have its associated vacancy cascade, meaning that the experimentally determined vacancy cascade will consist of several overlapping components that are similar in form but not necessarily in intensity or position. The unique width and shape we found for each vacancy cascade confirms that it contains several components.

Results

Morphological Characterization. Crystallinity and dimensional data were extracted from the XRD results, for each of the samples, using the instrument software (they are found in Figure 1 and Table 1). As can be seen, with the exception of FeO, the samples are very pure, with crystal dimensions in the tens of nanometers. The trace contaminants were *suggested* by the instrument software to account for the very small extraneous peaks almost invariably found in diffraction spectra, as well as improper peak height ratios; the present diffraction spectra are typical of what was found for these materials in previous studies.

The impurities present in FeO are expected. As seen in eq 2, and noted in our previous paper on Fe oxidation,[1] the surface of FeO is unstable to atmosphere, decomposing to Fe^0 and Fe_3O_4, both of which are capable of further oxidation. The atmospheric oxidation of Fe leads again to unstable FeO,[1] while that of Fe_3O_4, without a change in crystal structure, leads to γ-Fe_2O_3. The absences of both Fe^0 and Fe_3O_4 from the diffraction data indicate extensive surface layer decomposition and oxidation. Surprising findings are the suggested trace of Fe^0 present in both Fe_3O_4 and α-Fe_2O_3 (Table 1) and that of α-Fe_2O_3 present in Fe_3O_4 (rather than the expected γ-Fe_2O_3). The former may indicate that some of the Fe^0 used in preparing the oxides remained unoxidized, perhaps protected at the center of a particle; the latter (and, perhaps, the former as well) probably indicates the extent of reliability one can place on computer suggestions of extraneous peaks and improper peak ratios. However, these are trace amounts, not enough to vitiate the XPS results.

Particle size distributions were obtained for all the oxides. As seen for the case of γ-Fe_2O_3, in Figure 2, the spherical equivalent size distribution differs, depending on whether it is presented in terms of the number of particles, their volumes, or their surface areas; their mean values are found in Table 2. What is clear, however, is that a comparison of the crystal sizes, in Table 1, and the particle sizes, in Table 2, indicates that they differ by 2−3 orders of magnitude. This disparity is clarified by a consideration of the sample morphology, as seen by several examples: SEM photomicrographs of α-Fe_2O_3 and Fe_3O_4 are found in Figures 3 and 4, respectively. The low resolution images, in Figures 3a and 4a, show micrometer-sized particles (as found in Table 2) that, on higher magnification, are seen, in Figures 3b and 4b, to be composed of aggregated nanometer-sized particles (as shown in Table 1).

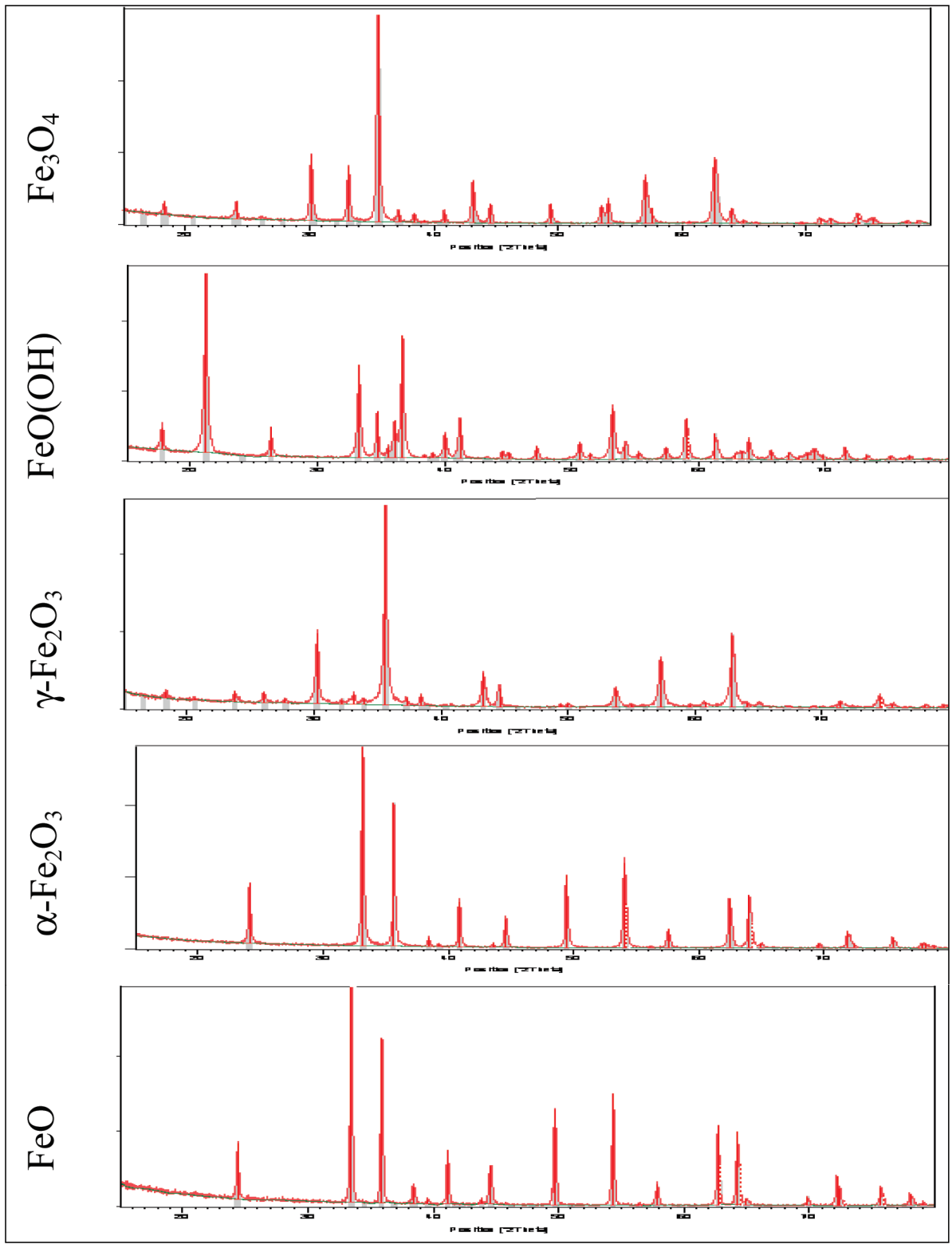

Figure 1. XRD diffraction patterns for the oxides used in this study.

TABLE 1: X-ray Diffraction Results

material	other materials present[a]	average crystal size (nm)
FeO	traces of Al[b], with a substantial amount of γ-Fe_2O_3	46
α-FeO(OH)	trace of Al[b]	84
Fe_3O_4	traces of Al[b], Fe, and α-Fe_2O_3	86
α-Fe_2O_3	traces of Al[b] and Fe	120
γ-Fe_2O_3	traces of Al[b] and α-Fe_2O_3	60

[a] Suggested by the instrument software. [b] From the sample holder.

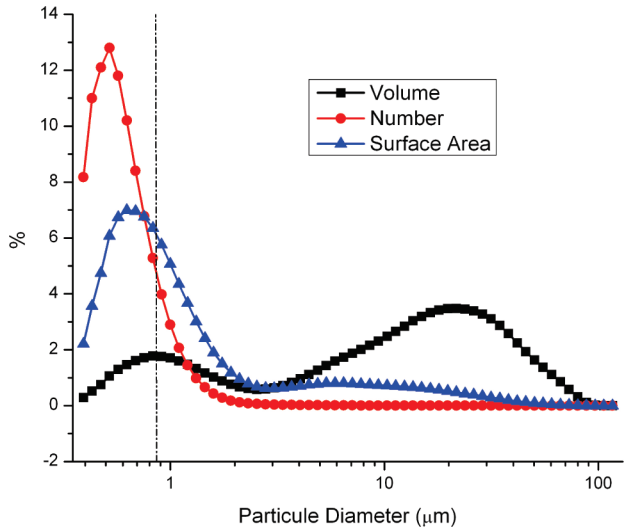

Figure 2. Particle size distributions for γ-Fe_2O_3: (a) volume %, (b) number %, and (c) area %.

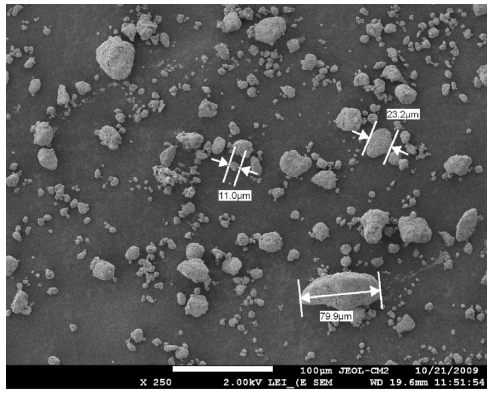

a

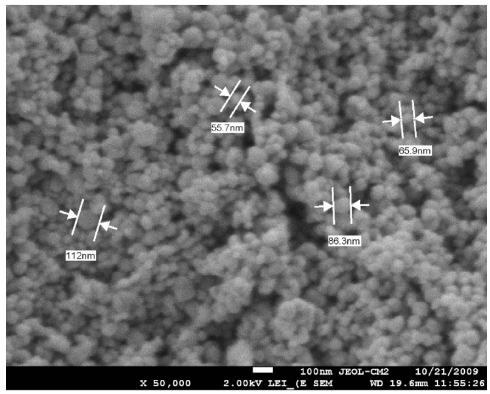

b

Figure 3. SEM photomicrographs of α-Fe_2O_3: (a) low resolution, showing the particles, and (b) high resolution, showing the NPs.

TABLE 2: Mean Particle Size Diameters

	mean particle size diameters (μm), as determined by		
material	volume %	number %	surface area %
FeO	320	0.8	75
α-FeO(OH)	1.4	0.6	1.0
Fe_3O_4	62	0.8	18
α-Fe_2O_3	75	0.7	11
γ-Fe_2O_3	17	0.7	3.0

XPS Characterization. As already noted in the Experimental Section, we adopted a particular philosophy for the separation of the spectra into their component peaks. For the O 1s spectrum,

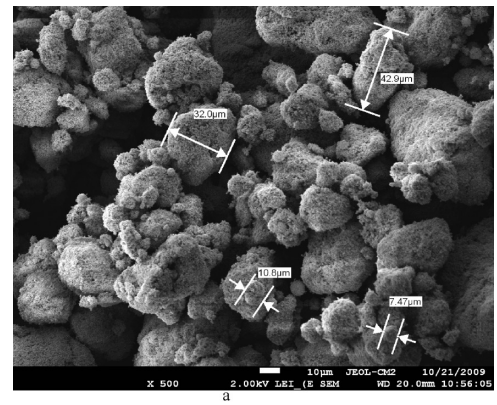

a

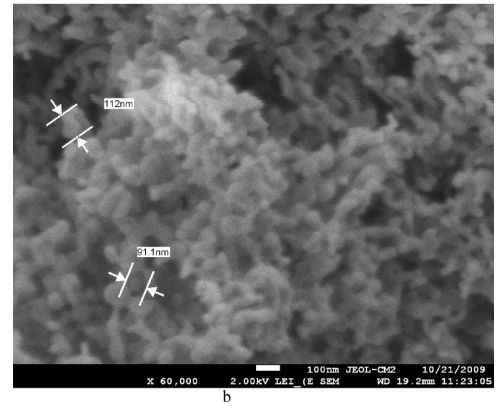

b

Figure 4. SEM photomicrographs of Fe_3O_4: (a) low resolution, showing the particles, and (b) high resolution, showing the NPs.

the component widths were maintained constant at 1.8 eV. As noted earlier, this is the value we had determined, on our instrument, over a period of 25 years, as applicable to both inorganic and organic materials.

In the case of the Fe $2p_{3/2}$ spectrum, no limits were placed on the symmetric component widths since it was expected that the peaks would be influenced by ligand field effects due to the Fe environment (i.e., tetragonal, octahedral), crystalline disorder at the NP surface, and Russell−Saunders coupling of Fe^{III}. In the case of Fe_3O_4, there are three Fe environments (Fe^{II} octahedral, Fe^{III} octahedral, Fe^{III} tetrahedral), and in the case of γ-Fe_2O_3, there are two (Fe^{III} octahedral, Fe^{III} tetrahedral). Not knowing the effect of environment on either ligand field effects or Russell−Saunders coupling, we felt it best to maintain the same width for each ion in each environment in a given sample. We are unaware of the error caused by this approximation, although our spectral fits indicate that they are probably not large.

It is evident that these contributions to the Fe $2p_{3/2}$ spectrum are different for each of the oxides studied, as the fwhm values necessitated by the analyses vary from 2.6 eV for γ-Fe_2O_3 to 4.6 for FeO(OH). Thus, while the contributions due to ligand field effects and Russell−Saunders coupling may be shown to influence the spectral widths used, they cannot presently be separated. Further, no effort was made to use more Fe 2p peaks in a spectrum than the minimum number required: that is, the number of peaks employed in any spectrum was determined solely by the shape of the spectrum and the number of symmetric peak components needed to fit it. Peak fits for the oxides, excluding FeO, which could not be characterized because of its surface instability,[1] are seen in Figure 5 and are summarized in Table 3. Although we have no idea of the morphologies of the samples used in prior studies, our spectra appear to be quite similar.

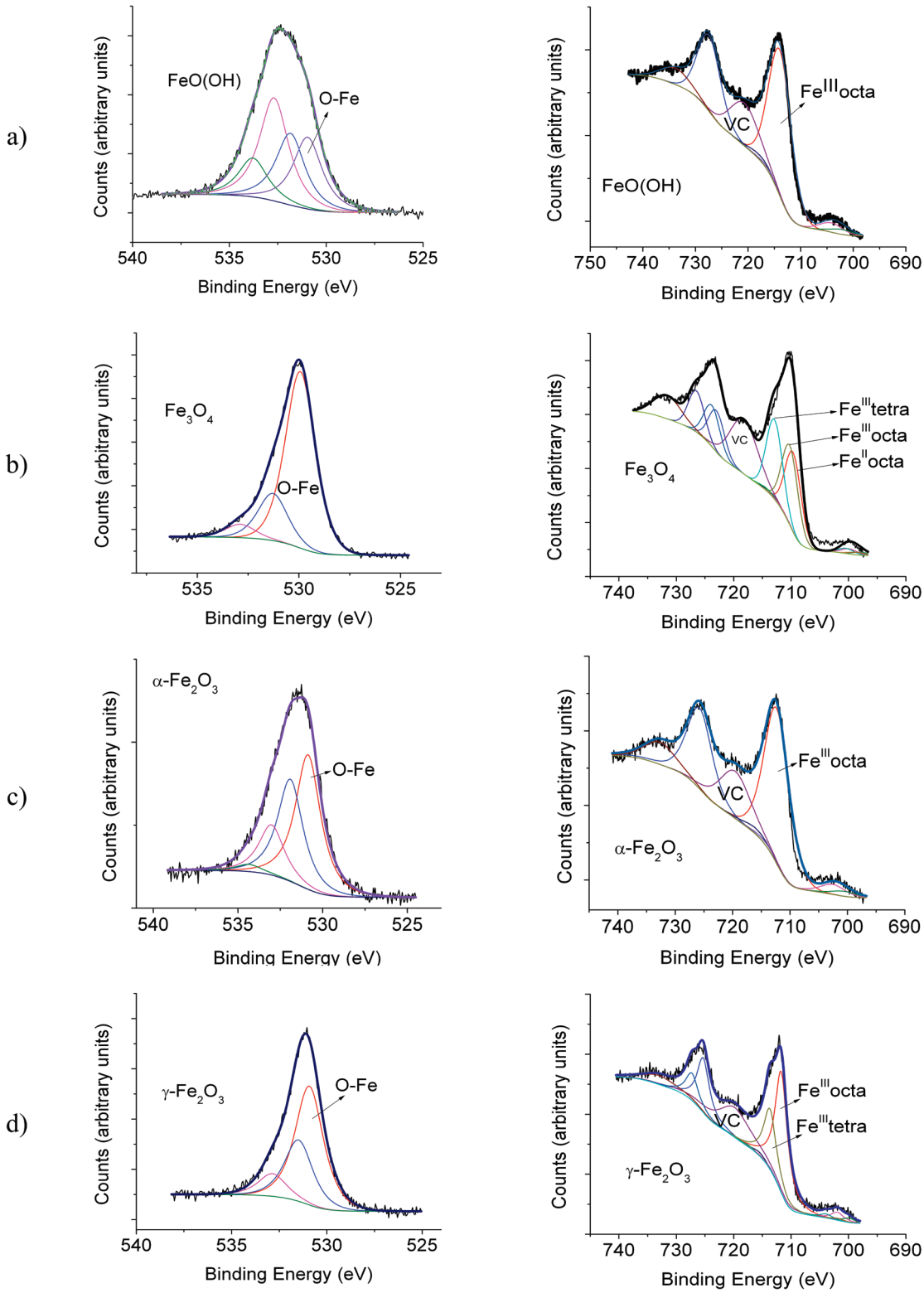

Figure 5. O 1s and Fe 2p peak fits are shown for (a) α-FeO(OH), (b) Fe_3O_4, (c) α-Fe_2O_3, and (d) γ-Fe_2O_3. These may be compared with those previously obtained for Fe^0 and its initial oxidation, which are found in ref 1 .

In these *initial* results, no attempt was made to account for crystalline disorder at the NP surface. As a result, a single O 1s peak, with a fwhm of 1.8 eV, was used for Fe−O bonding. Further, it was satisfying to note that, while no effort was made to use more Fe 2p component peaks than necessary, the expected Fe component peak ratios (say, the Fe^{III} octahedral:tetrahedral ratio for γ-Fe_2O_3) were *nearly* obtained on initial deconvolution (1.9:1 for γ-Fe_2O_3); when the ratio was then fixed to the value expected (precisely 2:1 for γ-Fe_2O_3), no deconvolution problems were encountered.

However, as seen in Table 3, the experimentally determined Fe:O ratios of α- and γ-Fe_2O_3, in particular, are not as close to the expected values as we would have anticipated. We chose to seek improvement in the following manner. Because there must obviously be a loss of crystalline order at the outer surfaces of the NPs, we decided to take this into account in the following

TABLE 3: Initial XPS Results

Material	Peak Position (eV)[a]	Attribution[b]	FWHM (eV)	Peak Ratio	Fe:O Ratio Expected	Fe:O Ratio Found
α-FeO(OH)	Fe: 713.9[c]	Fe^{III} octahedral	4.6	-	1:2	1:1.8
	O: 531.0	-O-Fe	1.8	1:1		
	531.9	-OH	1.8			
Fe_3O_4	Fe: 709.6	Fe^{II} octahedral	3.4	1:1:1	3:4	3:4.2
	710.2	Fe^{III} octahedral	3.4			
	712.9	Fe^{III} tetrahedral	3.4			
	O: 529.9	-O-Fe	1.8			
α-Fe_2O_3	Fe: 712.3	Fe^{III} octahedral	4.4		2:3	2:2.3
	O: 530.9	-O-Fe	1.8			
γ-Fe_2O_3	Fe: 711.7	Fe^{III} octahedral	2.6	2:1	2:3	2:2.6
	713.7	Fe^{III} tetrahedral	2.6			
	O: 530.9	-O-Fe	1.8			

[a] Multiple peaks were not used unnecessarily but only when dictated by the necessity to fill the asymmetric spectra with symmetric component peaks. [b] Fe attributions are from ref 1. [c] The higher energy of this Fe^{III} octahedral peak is due to the −OH inductive effect. Its value was excluded from the binding energy averaging in the Discussion.

TABLE 4: Improved Fe:O Ratio for α-Fe_2O_3

	O 1s Peak Position (eV)	Attribution	Peak Ratio	Fe:O Ratio
initial:	530.9	crystalline		2:2.3
Improved:	530.0	disordered	0.074:1	2:3.1
	531.1	crystalline		

manner: a loss of crystalline order translates as a loss of Fe−O orbital overlap, making the Fe atom more positive and the O atom more negative. If this were so, one would expect an additional O 1s peak component shifted to a slightly lower binding energy and, in a similar fashion, additional Fe 2p peak components shifted to slightly higher binding energy.

To test this assumption, the peak separation software was programmed to add another O 1s peak for each of the oxides, without specifying where. In each case, the peak added by the program was placed at a binding energy *below* the previously existing Fe−O peak, as would be expected for a loss of orbital overlap. In the case of the Fe 2p spectrum, our inability to separate this effect from the Fe−O environment effect and Russell−Saunders coupling, as mentioned earlier, means that this was already (unintentionally) accounted for in our initial peak separations.

Thus, our only test of the effect of crystalline disorder can be made on the O 1s spectrum. An example is seen in Table 4, where the results for α-Fe_2O_3, which gave the worst Fe:O ratio in Table 3 (Fe:O = 2:2.3, with 2:3 expected), gave an *improved* ratio of 2:3.1 after a second peak was added to the O 1s spectrum. Indeed, although the improvement in the Fe:O ratio for α-Fe_2O_3 is by far the most dramatic, similar improvements were found for all the other oxides. The addition invariably improved the fitting statistics (as it must, even if it were not required). In each case, the new Fe−O bonding peak invariably appeared at a lower binding energy than the initial Fe−O bonding peak, and in every instance, the ratio of the new peak to the initial peak lay in the range 0.05:1 to 0.074:1. That is, the crystal surface imperfection estimated in this manner is found to be in the range of 5−7% of the volume probed for all the oxides in this study. As seen in Figures 3b and 4b, the NPs are spherical, with average diameters in the 100 μm range. In comparison, the values we found for the new peaks are of the same order of magnitude as the disordered surface layer proposed by Buffat and Borel[20] to explain the lowering of the melting point of Au NPs with decreasing size, by Kofman et al.[21] for a similar effect occurring in Pb NPs, and by Sun et al.[22] in their melting point-size correlations of several NPs.

Discussion

Ligand Field Effects on Peak Positions. In our previous paper on the characterization of Fe nanoparticles,[1] we found that, on exposure to O_2, Fe formed several oxidation products, in a mechanism described by eqs 1−3. During the initial oxidation process, Fe^0 formed FeO, which decomposed into Fe^0 and Fe_3O_4 (magnetite); the reformed Fe^0 began the oxidation process again, while the Fe_3O_4 oxidized further, without a change in crystal structure, to form γ-Fe_2O_3 (maghemite). Thus, until the Fe^0 is exhausted, one should be able to find peaks in the Fe 2p spectrum representative of the three oxides. In fact, we found that the oxidation products could be represented by four peaks, which were referred to as C_1−C_4 (see ref 1 for details), at ∼709, ∼ 710, ∼711, and ∼712 eV, respectively. Basing ourselves on (1) our previous results[2] on the Co 2p XPS peak positions of Co^{II} and Co^{III} in the spinel-structured Co_2O_3, (2) our expectation that the nuclear charge on Fe^{III} of a given crystal structure should cause photoemission at a higher binding energy than Fe^{II} with the same crystal structure, and (3) our understanding of the differences in orbital overlap in octahedral and tetrahedral environments,[1] we were led to the *tentative conclusion* (so noted in ref 1) that C_1−C_4 could be attributed,

respectively, to Fe^{II} (rock salt structure in FeO), Fe^{II} (octahedral), Fe^{III} (octahedral), and Fe^{III} (tetrahedral).

Except for FeO, whose surface we found to be heavily oxidized in our sample, and which could not be used to verify the binding energy of the Fe^{II} (rock salt) peak, the use of high purity Fe oxide standards in the present study has permitted us to verify the peak positions of the other attributions. Table 3 indicates that Fe^{II} (octahedral) appears at 709.6 eV (there is only one such peak in Table 3), Fe^{III} (octahedral) at 710.2−711.7 eV (the peak for FeO(OH) was omitted from the averaging because of different charges on the different oxygen atoms[23]), and Fe^{III} (tetrahedral) at 712.9−713.7 eV. These are to be compared with the positions of C_2−C_4 used in our previous study: ∼710, ∼711, and ∼712 eV. We note, with satisfaction, that the order of the peaks we originally proposed[1] is seen to be confirmed by the present results. Given the facts that (1) the C_1−C_4 peak positions were originally[1] determined by assuming the same fwhm value for all the Fe 2p peaks (inaccurate, as seen in Table 3), (2) the C_1−C_4 peak positions were determined for trace oxides,[1] which gave small peaks that were difficult to separate, and (3) the determinations of the present peak positions are complicated by the presence of contaminants and crystalline disorder, the energy correspondence appears to be reasonable.

Presence of Crystalline Surface Disorder. In 1927, Goldschmidt pointed out[24] that, at the surface of a crystal, the coordination with other atoms is lost, and the ionic radius contracts, producing a surface disorder. As we noted earlier, this concept was invoked by several research groups[20−22] to explain the melting behavior variation with crystal size found in NPs. Our group, together with that of Yacamán,[18] demonstrated, with high resolution TEM photomicrographs, that surface disorder is observable in NPs and plays a fundamental role in their surface diffusion and coalescence.

It is our contention that the presence of surface disorder manifests itself in our spectra. While, as we have explained, the presence of several simultaneous phenomena (surface disorder, ligand field effects, and Russell−Saunders coupling) prevents our demonstration of surface disorder in the Fe 2p spectrum, this is not the case for the O 1s spectrum. There, we base ourselves on the fact that, since the inception of our laboratory in 1984 with its VG ESCALab 3 Mk II spectrometer, the width of the O 1s peak, in many different environments, has always been found to be 1.8 eV.[1,2,19,25−35] We have thus found it possible to separate oxygen environments when several exist in a sample, whether organic or inorganic. It is for this reason that we undertook to explore the introduction of an additional O 1s peak in our oxide samples. The results are gratifying (Table 4): not only is the fit improved but also the new peak appears at a binding energy lower than that of the ordered peak, and its intensity is consistent with what is expected for a disordered surface layer. This is strong support for our position.

Contribution of Vacancy Cascades. As noted in our previous paper,[1] remarkably similar sequences of Auger electron and photon emissions (vacancy cascades) were calculated for Fe^0 and its ions,[13,14] accounting for the similar 2p peak shapes that have been found for Fe^0, its halides, and oxides.[36] This is so, despite the fact that each ion, in its own environment in our oxides (i.e., Fe^{II} octahedral, Fe^{III} octahedral, and Fe^{III} tetrahedral in Fe_3O_4), contributes its own overlapping vacancy cascade component. In fact, because of different ions and environments for each of the oxides, such an overlap is expected to produce somewhat different shapes of the vacancy cascade contribution for each oxide, resulting in spectra peaking at slightly different binding energies with slightly differing forms and having different inflection points. Such differences would then confirm that the experimental peak is composed of overlapping components.

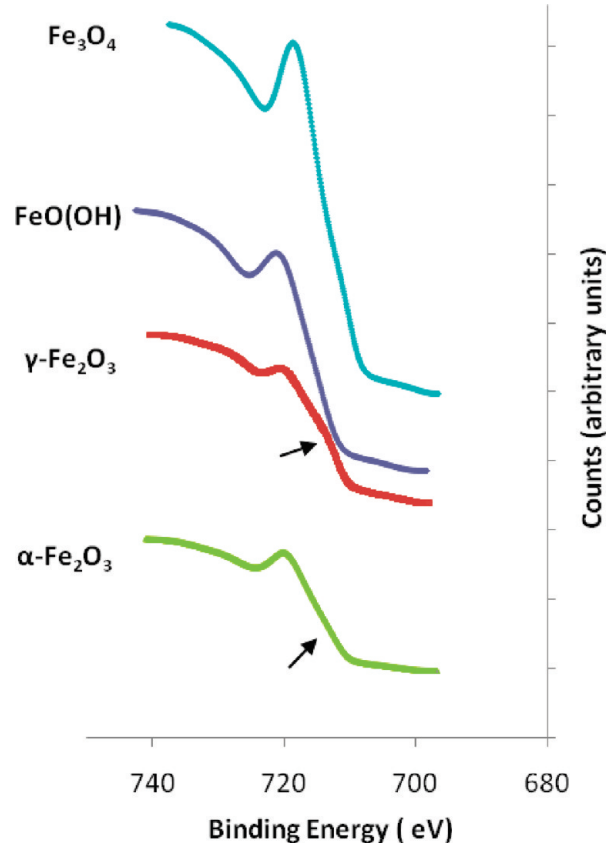

Figure 6. Vacancy cascades for the oxides. The arrows indicate obvious inflection points, showing shape differences among the vacancy cascade processes.

We verify this, using our own data. The vacancy cascades of all the oxides, with the exception of FeO, are found in Figure 6, where the vacancy cascades of the Fe 2p spectra in Figure 5 are displayed. There, it is seen that the peak shapes, while similar, are, indeed, displaced in binding energy; some, such as α- and γ-Fe_2O_3, even have very obvious shoulders (indicated by arrows), demonstrating the presence of overlapping components. This correspondence, to what is expected for multiple vacancy cascade component overlap, supports our original contention[1] that the asymmetry found in the 2p spectra of Fe^0 and its ions has a vacancy cascade component.

Conclusions

High purity Fe oxide nanoparticulate samples have been used to reveal that their Fe 2p XPS spectra may be separated into several expected contributions, using symmetrical component peaks. In carrying out such separations, account is taken of the ligand field environment, nanoparticle surface disorder, and Fe^{III} Russell−Saunders coupling. The vacancy cascade components of the Fe 2p spectra have been shown to be similar in form yet different enough in peak position and shape to indicate that their makeup is due to the expected overlapping contributions from all the Fe environments present in the nanocrystals.

Acknowledgment. We thank the Natural Sciences and Engineering Research Council of Canada and NanoQuébec for

funding, and Arthur Yelon for his advice on the presentation of the present data.

References and Notes

(1) Yang, D.-Q.; Sacher, E. *J. Phys. Chem. C* **2009**, *113*, 6418.
(2) Zhang, G.-X.; Yang, D.-Q.; Sacher, E. *J. Phys. Chem. C* **2007**, *111*, 17200, and references therein.
(3) McIntyre, N. S.; Zetaruk, D. G. *Anal. Chem.* **1977**, *49*, 1521.
(4) Fujii, T.; de Groot, F. M. F.; Sawatsky, G. A.; Voogt, F. C.; Hibma, T.; Okada, K. *Phys. Rev. B* **1999**, *59*, 3195.
(5) Aronniemi, M.; Lahtinen, J.; Hautojarvi, P. *Surf. Interface Anal.* **2004**, *36*, 1004.
(6) Grosvenor, A. P.; Kobe, B. A.; Biesinger, M. C.; McIntyre, M. S. *Surf. Interface Anal.* **2004**, *36*, 1564.
(7) Prince, K. C.; Matteucci, M.; Kuepper, K.; Chiuzbaian, S. G.; Bartkowski, S.; Neeumann, M. *Phys. Rev. B* **2005**, *71*, 085102.
(8) Yamashita, T.; Hayes, P. J. J. *Electron Spectrosc. Relat. Phenom* **2006**, *152*, 6. Paparazzo, E. J. *J. Electron Spectrosc. Relat. Phenom.* **2006**, *154*, 28. Yamashita, T.; Hayes, P. J. *J. Electron Spectrosc. Relat. Phenom.* **2006**, *154*, 41.
(9) See http://srdata. nist.gov/xps/ElmComposition.aspx (NIST XPS Data Base), where the elements Fe and O should be selected.
(10) Gupta, R. P.; Sen, K. S. *Phys. Rev. B* **1974**, *10*, 71. Gupta, R. P.; Sen, K. S. *Phys. Rev. B* **1975**, *12*, 15.
(11) Doniach, S.; Šunjić, M. *J. Phys. C: Solid State Phys.* **1970**, *3*, 285. Gadzuk, W.; Šunjić, M. *Phys. Rev. B* **1975**, *12*, 524.
(12) Cooper, E, P. *Phys. Rev.* **1942**, *61*, 1.
(13) Jacobs, V. L.; Davis, J.; Roszynai, B. F.; Cooper, J. W. *Phys. Rev. A* **1980**, *34*, 1917.
(14) Jacobs, V. L.; Davis, J.; Roszynai, B. F. *Phys. Rev. A* **1986**, *34*, 1216.
(15) http://wwwchem.uwimona.edu.jm/courses/RScoupling.html.
(16) Briggs, D.; Seah, M. P. *Practical Surface Analysis*; Wiley: New York, 1983; Chapter 3.2.2.
(17) Huheey, J. E. *Inorganic Chemistry*, 2nd ed.; Harper & Row: New York, 1978.
(18) José-Yacamán, M.; Gutierrez-Wing, C.; Miki, M.; Yang, D.-Q.; Piyakis, K. N.; Sacher, E. *J. Phys. Chem. B* **2005**, *109*, 9703, and references therein.
(19) Sacher, E.; Klemberg-Sapieha, J. E. *Phys. Rev. B* **1989**, *39*, 1461, our study of the spectral decomposition of the similar p−d splitting of Cu in CuO.
(20) Buffat, Ph.; Borel, J.-P. *Phys. Rev. A* **1976**, *13*, 2287.
(21) Kofman, R.; Cheyssac, P.; Aouaj, A.; Lereah, Y.; Deutscher, G.; Ben-David, T.; Pennison, J. M.; Bourret, A. *Surf. Sci.* **1994**, *303*, 231.
(22) Sun, C, Q; Wang, Y.; Tay, B. K.; Li, S.; Huang, H.; Zhang, Y. B. *J. Phys. Chem. B* **2002**, *106*, 10701, and references therein. Sun, C. Q.; Tay, B. K.; Zeng, X. T.; Li, S.; Chen, T. P.; Zhou, J.; Bai, H. L.; Jiang, E. Y. *J. Phys.: Condens. Matter* **2002**, *14*, 7781, and references therein. See ref 18 for further details.
(23) Ding, M.; De Jong, B. H. W. S.; Roosendahl, S. J.; Vredenberg, A. *Geochim. Cosmochim. Acta* **2000**, *64*, 1209; see Table 1 and the associated text.
(24) Goldschmidt, V. M. *Ber. Dtsch. Chem. Ges.* **1927**, *60*, 1270. See also: Feibelman, P. J. *Phys. Rev. B.* **1996**, *53*, 13740. Kara, A.; Rahman, T. S. *Phys. Rev. Lett.* **1998**, *81*, 1453. Sun, C. Q. *Prog. Solid State Chem.* **2007**, *35*, 1.
(25) Lachkar, A.; Selmani, A.; Sacher, E.; Leclerc, M. *Synth. Met.* **1995**, *72*, 81.
(26) Sacher, E.; Kemberg-Sapieha, J. E. *J. Vac. Sci. Technol. A* **1997**, *15*, 2143.
(27) Sandrin, L.; Sacher, E. *Appl. Surf. Sci.* **1998**, *135*, 339.
(28) Popovici, D.; Sacher, E.; Meunier, M. *J. Appl. Polym. Sci.* **1998**, *70*, 1201.
(29) Yang, D.-Q.; Poulin, S.; Sacher, E.; Hyett, C. *Appl. Surf. Sci.* **2000**, *165*, 116.
(30) Yang, D.-Q.; Sacher, E. *Appl. Surf. Sci.* **2001**, *173*, 30.
(31) Yang, D.-Q.; Martinu, L.; Sacher, E.; Sadough-Vanini, A. *Appl. Surf. Sci.* **2001**, *177*, 9703.
(32) Yang, D.-Q.; Sacher, E. *Appl. Surf. Sci.* **2002**, *195*, 202.
(33) Yang, D.-Q.; Rochette, J.-F.; Sacher, E. *J. Phys. Chem. B* **2005**, *109*, 7788.
(34) Zhang, G.-X.; Yang, D.-Q.; Sacher, E. *J. Phys. Chem.C* **2007**, *111*, 565.
(35) Yang, D.-Q.; Rochette, J.-F.; Sacher, E. *J. Phys. Chem. B* **2008**, *112*, 4075.
(36) See, e.g.: Grosvenor, A. P.; Kobe, B. A.; Biesinger, M. C.; McIntyre, N. S. *Surf. Interface Anal.* **2004**, *36*, 1564.

JP100964X